A Method for Generating Desired Contact Pressure Distributions in Experimental Interfacial Studies[1]

M. H. Attia
Tribology and Mechanical Processes Unit,
Ontario Hydro Research,
Toronto, Ontario, Canada
Assoc. Mem. ASME

L. Kops
Assoc. Professor,
Department of Mechanical Engineering,
McGill University,
Montreal, Quebec, Canada
Mem. ASME

Computer simulation of the thermal deformation behavior of machine tools requires a priori knowledge of the correlation between the contact pressure distribution and the thermal contact resistance distribution along the structural joint. To establish this correlation experimentally, a method for generating different distributions of contact pressure has been devised in the present work. The method provides also a basic tool toward the satisfaction of the requirements of simulative wear testing.

In this paper, the effect of the relative flexural rigidity of two solids in contact on the shape of the distribution of contact pressure is presented as a means for generating desired contact pressure distributions. The theoretical background of the concept is discussed considering two limiting cases: a rigid body on an elastic semi-infinite mass, and an elastic layer on a rigid base. Through a photoelastic analysis, the geometric parameters of contacting bodies, which allow us to generate the desired distributions, have been defined. The results of the analysis were verified by a two-dimensional, plane-stress finite element model.

The results indicated that a finite plate, whose dimensions are not less than three-fold the contact length can simulate a two-dimensional rigid base or a semi-infinite elastic mass. A change in the height-to-contact length ratio of the contacting beam from 0.5 to 2.5, causes a significant change in its elastic response from a flexural to a rigid body.

Introduction

The nonuniformity in the distribution of the contact pressure between the components of a machine tool structure is inherent to its design and functional requirements. As the data available in the open literature demonstrate [1-5], the profile of this distribution reflects the influence of the mechanical and thermal load on the parameters which characterize the stiffness of contacting structural elements. These parameters are the geometric configuration, the mechanical properties, and the surface topography.

It is a well-known fact that machining errors due to thermal deformation of machine tool structures are comparable in magnitude to those resulting from tool wear and mechanical deflection. The effect of the distribution of the contact pressure on the thermal deformation of machine tools was first recognized by the authors in [6]. Through the changes in the local values of the thermal contact resistance, the distribution of the contact pressure plays a significant role in controlling the temperature field in the structure [7]. According to the theory of nonlinear thermoelastic behavior of structural joints [8], thermal deformation resulting from the temperature field develops thermal contact stresses along the joint, which alter existing contact pressure distribution. This activates a thermo-mechanical, closed-loop interaction at the joint, which proceeds until the state of equilibrium between all parameters taking part in the process has been reached.

The significant effect of the interactions at the joint on the thermal deformation behavior of the structure, and consequently the machining accuracy, has been demonstrated in [9, 10] and supported by experimental evidence [11].

To predict the thermal deformation of the machine tool structure, with the nonlinear thermoelastic behavior of the joint is taken into account, a computer simulation scheme has been developed [12]. A key element in this scheme is the preknowledge of the correlation between the distributions of the contact pressure and the thermal contact resistance. This requirement called for the replacement of the existing method of measuring the thermal contact resistance as a mean value by a new method, in which the thermal contact resistance is measured as position-dependent for a known contact pressure distribution along the interface [13]. The concept of generating various distributions of contact pressure for that purpose, based on the theory of unbonded contact of beams on elastic foundation, has been outlined in [13] and is the subject of detailed analysis in the present paper.

The concept and the results presented in this study are neither restricted to machine tool joints, nor confined to the problem of thermal contact resistance. In the area of tribology, the need for a method for generating desired contact pressure distributions for simulative wear testing has

[1] This paper is based on a research work carried out at McGill University.

Contributed by the Production Engineering Division for publication in the JOURNAL OF ENGINEERING FOR INDUSTRY. Manuscript received at ASME Headquarters, November 16, 1984.

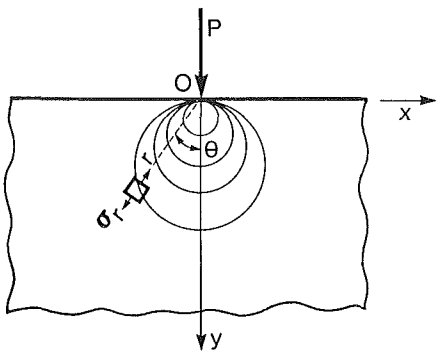

Fig. 1 A concentrated line load (distributed along z-axis) acting on an elastic semi-infinite body – radial stress field (isochromatic lines)

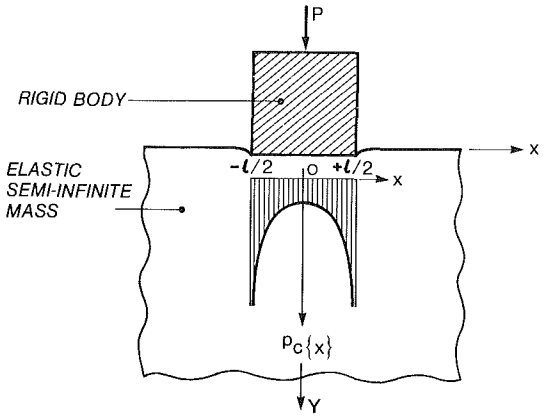

Fig. 2 Contact pressure distribution at the interface of a rigid body on an elastic semi-infinite mass under the influence of a concentrated line load

been recognized. This need stems from the established correlation between the distribution of the contact stresses and the wear process. The extent and the location of the fretting wear damage, for example, cannot be predicted without a priori knowledge of the distribution of the contact stresses. Supported by experimental evidence, examples for coupling the contact stress solution and the wear formulation were presented in [14–17].

Toward improving the applicability of laboratory wear tests in practice, the similarity theory dictates that the characteristic stress in the model and the original structure should be the same [18]. The characteristic stress, which decisively acts on the wear process, varies according to the wear mechanism. In the case of layer wear, e.g., it is the maximum contact pressure and not the mean value that should be reproduced. Therefore, there is a need to create the proper distribution of the contact pressure in the model to account for various types of loading which act on the actual structure (mechanical, thermal, and residual stresses) [18]. In the current tribological research programs in West Germany [19, 20], contact stresses have been recognized as one of the quantities to be measured in practice-oriented laboratory testing.

The experimental study carried out by Rice [21], under sliding and impact wear conditions, concluded that the phenomenological wear behavior and the wear track profile depend not only on the nominal (average) contact stress, but also on the stiffness of the specimens. This indicates that it is the distribution of the contact pressure and not its average value that controls and characterizes the wear process. The theoretical analysis carried out by Fedotova [22] supports this conclusion.

The interpretation of the wear process as a result of subsurface fracture, provided a theoretical background for the effect of the distribution of the contact pressure, which defines the local microscopic contact conditions, on the wear rate and the nature of particle detachment [23, 24].

The Concept of Generating Different Distributions of Contact Pressure – Theoretical Background

The concept adopted in the present study, to generate different distributions of contact pressure, is based on the dependence of the latter on the relative flexural rigidity of the solids in contact. The external loading is confined to the case of a concentrated line load, due to the uncertainty associated with the practical application or measurement of any other type of loading. An appreciation of this concept can be gained by considering the following two limiting cases: a rigid body on an elastic semi-infinite mass and an elastic layer resting on a rigid base.

A Rigid Body on an Elastic Semi-Infinite Mass. The response of the surface of a semi-infinite mass to contact pressure exerted by a rigid body can be constructed from Michell's classical analysis of a concentrated load acting on

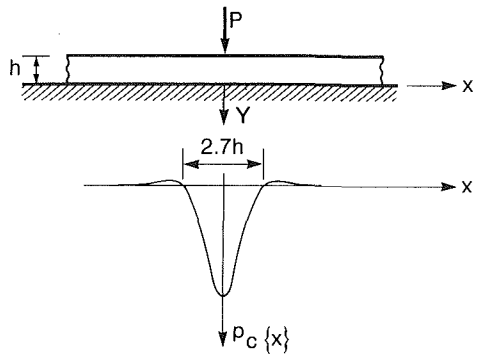

Fig. 3(*a*) An infinitely long rectangular beam

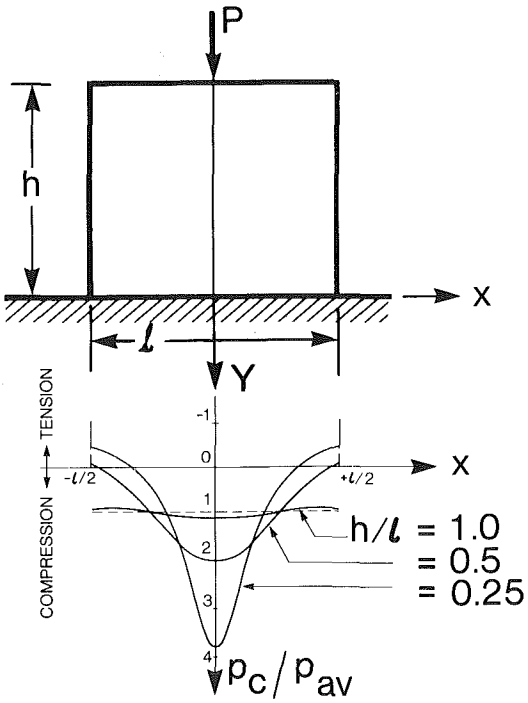

Fig. 3(*b*) A rectangular beam of finite length

Fig. 3 Contact pressure distribution at the interface of an elastic body (beam) resting on a rigid base under the influence of a concentrated line load

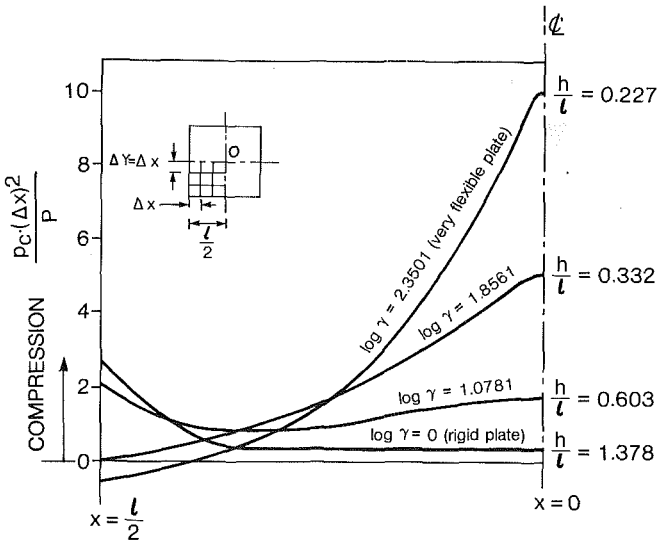

Fig. 4 Contact pressure distribution along the centerline of a square plate on a semi-infinite mass under a central concentrated load P [11]

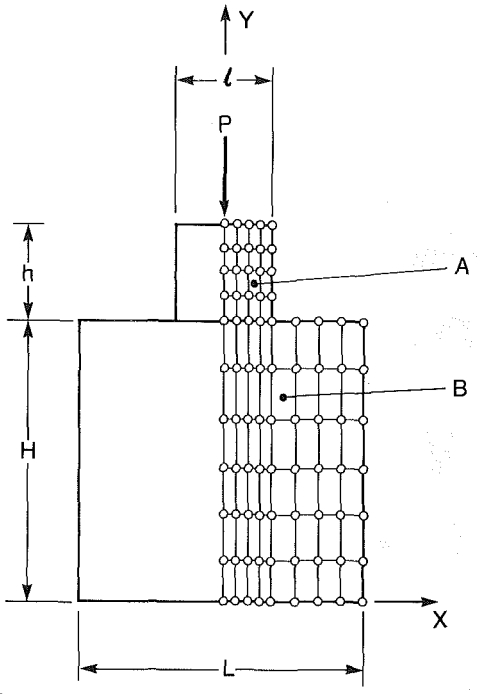

Fig. 5 Two dimensional model composed of plates A and B – finite element idealization

the boundary of a mass. In two-dimensional configurations (Fig. 1), where the mass is substituted by a large plate of a unit thickness, the stresses acting on an infinitesimal element at a distance r from the applied concentrated line load P is a simple compressive radial stress σ_r [25]:

$$\sigma_r = \frac{-2P\cos\theta}{\pi r} \tag{1}$$

$$\sigma_\theta = \tau_{r\theta} = 0 \tag{2}$$

where σ_θ and $\tau_{r\theta}$ are the tangential and shear stresses, respectively, and P is the load per unit thickness.

Along any circle having its center on the y-axis and passing through the point of load application 0, σ_r is constant except at point 0 where it becomes infinity. Knowing the stress field, the vertical displacement along the surface of the semi-infinite mass is expressed as:

$$\left[v\right]_{\theta=\pm\frac{\pi}{2}} = \pm\left[\frac{2P}{\pi E}\cdot\log\frac{d}{r} - \frac{(1+\nu)}{\pi E}P\right] \tag{3}$$

where d is the depth of a point, located on the y-axis, which does not move vertically. The principal superposition permits the use of the influence lines obtained from Michell's solution to determine the displacements at any point in the elastic body under any arbitrary load distribution.

The displacement of the free boundary $y=0$ due to a surface traction $p\{\xi\}$ acting over a portion of the boundary $a<x<b$ is:

$$v\{x\} = \frac{-2}{\pi E}\int_{\xi=a}^{\xi=b} p\{\xi\}\log|x-\xi|d\xi \tag{4}$$

where $|x-\xi|$ represents the positive distance between the load element $p\{\xi\}$ at ξ and the point of observation at x.

When the concentrated load is transmitted to the elastic mass through a rigid body of a length l, the deflection along this portion of the boundary will be constant. Sadowsky's solution [26] for the contact pressure distribution $p_c\{x\}$ which produces this type of surface deflection is expressed as:

$$p_c\{x\} = \frac{2P}{\pi\sqrt{l^2-4x^2}} \tag{5}$$

Equation (5) indicates that while the contact pressure approaches infinity underneath the edges at $x=\pm l/2$, it attains a minimum value of $2P/\pi l$ at $x = 0$, as presented schematically in Fig. 2.

An Elastic Layer on a Rigid Base. It is pertinent to consider the solution of the classical problem of a finite long beam, of a thickness 2 h, subjected to collinear equal and opposite concentrated line loads P acting on both edges.

The middle plane of symmetry is free from shear stresses and vertical displacement, and therefore, the stress field within either half of the beam is equivalent to that produced in an elastic layer resting on a rigid base. The distribution of the vertical stresses σ_y along the middle plane $y=0$ (or equivalently, the contact pressure distribution $p_c\{x\}$) is given in [27-29].

Coker et al.'s solution [29] is presented schematically in Fig. 3(*a*). While attaining its maximum level underneath the point of application of the load $x=0$, the contact pressure diminishes, however, very rapidly with x and becomes zero at $x/h=1.35$.

At this point it is of interest to compare Figs. 2 and 3(*a*) to observe how the change in the relative rigidity of contacting solids would invert the shape of the contact pressure distribution. It seems, also, reasonable to predict that an increase in the rigidity of the elastic beam would bridge the transition between these two contact pressure profiles, passing through a critical value which corresponds to a uniform pressure distribution. This prediction is supported by the results reported by Goodier [27] and Theocaris [30], for the case of a rectangular block, and a semi-infinite strip subjected to a concentrated line load, respectively. The change in the distribution of $[\sigma_y]_{y=0}$ as the height of the beam h is increased with respect to the contact length l is presented schematically in Fig. 3(*b*) [27].

In the present study, an attempt is made to vary the relative rigidity of two contacting solids, made of the same material but of different cross-sections, by changing the height-to-length ratio h/l of the smaller body while maintaining the dimensions of the second unchanged (Fig. 5). Cheung et al. [31] applied the finite element method to determine the contact pressure distribution, along the centerline of a square plate resting on a semi-infinite body, under the influence of a concentrated load acting at the center of the plate. This particular configuration, and the type of loading as well, differs from the model investigated in the present study. Nevertheless, Cheung's results (Fig. 4) provide an indication

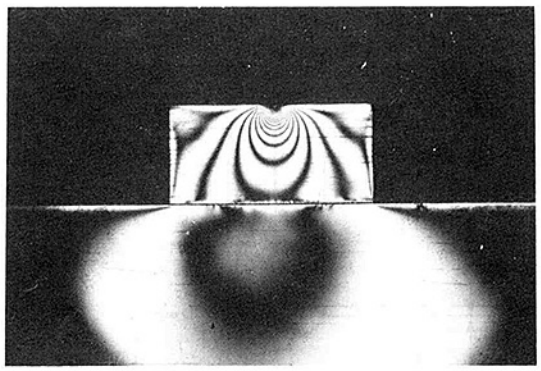

Fig. 6(a) $H/l = 0.5$

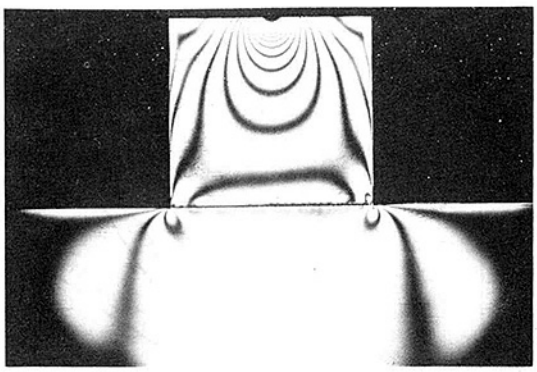

Fig. 6(b) $h/l = 1.0$

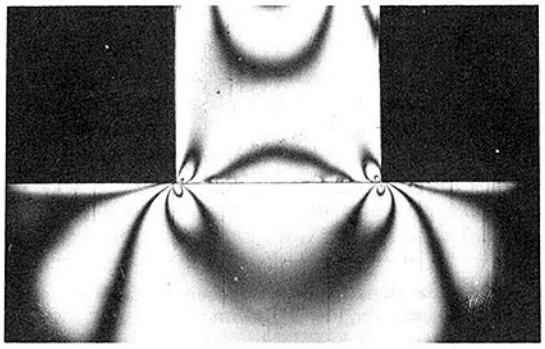

Fig. 6(c) $h/l = 1.5$

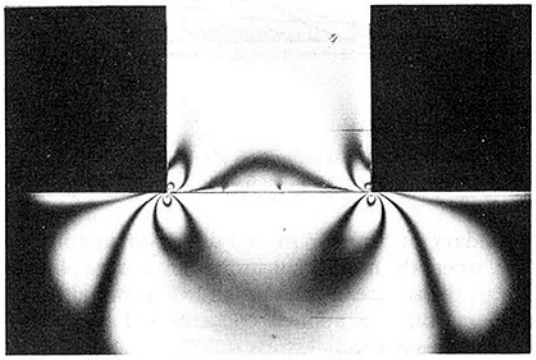

Fig. 6(d) $h/l = 2.5$

Fig. 6 Stress fringe pattern at the contact zone of two bodies (A and B) of different flexural rigidity when the smaller body A has a height-to-contact length ratio of

for the sensitivity of the system relative rigidity to the change in the height-to-length ratio h/l of the plate. An expression for the elastic response of such a system has been defined as:

$$\gamma = \frac{180\pi \cdot (\Delta x)^2 \cdot (\Delta y)}{h^3} \frac{1-\nu_p^2}{1-\nu_m^2} \cdot \frac{E_m}{E_p} \tag{6}$$

where E_p, E_m, and ν_p, ν_m are the moduli of elasticity and Poisson's ratios of the plate and the elastic mass, respectively. Δx, Δy are the dimensions of any of the rectangular finite elements, from which the plate is assembled, while h stands for the plate height. For this particular configuration, Fig. 4 shows that the two limiting cases (very flexible-, and absolutely rigid-plate) were achieved, as the h/l ratio of the plate varies only from 0.23 to 1.38, when both solids are made of the same material.

Photoelastic Analysis

A photoelastic analysis has been carried out to determine the dimensions of the two specimens in contact (A and B in Fig. 5), which render the relative rigidity of the system in a suitable range for generating different distributions of contract pressure. Specifically, the analysis was aimed at answering the following two questions:

– What are the minimum dimensions of the larger specimen to simulate an elastic semi-infinite plate/a rigid base?, and

– What height-to-contact length ratios h/l are to be chosen for the smaller specimen to behave as a rigid body/flexible beam, respectively?

The solution of the contact problem by the photoelasticity method, where plastic material is used, raises a question on the effect of the material elastic constants on the stress field. In other words, the validity of extrapolating the measurement results to other materials. Michell's theorem [32, 33] asserts that when a homogeneous and isotropic elastic body is in a state of either plane strain or generalized plane stress induced by prescribed surface tractions, the in-plane stresses do not depend on the elastic constants of the material, provided that such a body is simply connected. For the plane contact problem where the bodies are strained by mixed conditions at the surface, Dundurs et al. [3] have indicated that Michell's theorem is still valid, provided that certain conditions are met: the bodies are made of the same material, the contact surfaces are smooth, and the apparent contact area established by the geometries before loading stay either the same, or contract during loading. In the current study, these requirements were fulfilled, as the experimental setup is restricted to stationary contacts, in which the apparent contact area remains unchanged during loading.

Experimental Setup. The typical model shown in Fig. 5 consists of two plates A and B in contact. Both plates were cut to size from 1/4 in. (6.35 mm) thick photoelastic flat epoxy sheet (PSM-5, manufactured by Photoelastic Inc.). Using aluminum templates, the plastic models were first milled and then ground to the nominal dimensions (±0.075 mm) in accordance with the manufacturer's recommendations. Before loading, all models were checked photoelastically to ensure their freedom of residual stresses due to machining.

An optical bench-type transmission polariscope was used. Through a dead weight and cantilever arrangement, the model was subjected to a constant concentrated line load (over a length $l = 7.5$ mm) along the plane of symmetry. The material fringe constant was determined by averaging the results obtained from a circular disc-calibration model [34].

Experimental Procedure. By arranging the polariscope to produce a plane-polarized light field, the black bands of the isoclinic lines were recorded for different angular positions of the coupled polarizer-analyzer filter system. With the polariscope set as a circular polariscope, the polarized light from the stresses model produces the isochromatic fringe patterns shown in Figs. 6(*a*) to 6(*d*). The interference bands are proportional to the principal stress differences $(\sigma_x - \sigma_y)$:

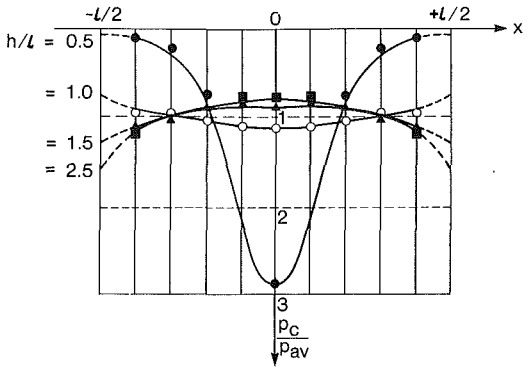

Fig. 7 Effect of the h/l ratio on the distribution of the contact pressure generated at the interface of the model shown in Fig. 5 – photoelastic results

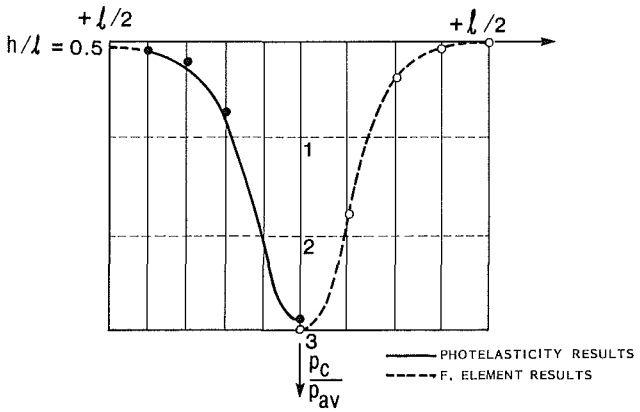

Fig. 8 Comparison of the contact pressure distribution results obtained by photoelasticity and finite element analysis, for $h/l = 0.5$

$$\sigma_x - \sigma_y = f \cdot \frac{N}{t} \tag{7}$$

where f is the material fringe constant, t is the thickness of the model while N stands for the number of the fringe order. The fringe order was established by comparing the isochromatic fringe pattern obtained as black and white, and as colored; the black line in both cases is the zero line. This was confirmed with the satisfaction of the condition of zero principle stresses, and consequently zero fringe order, at the external corners. Given the isoclinic parameter at the point under consideration, the Tardy method of compensation was used to determine the fractional fringe order to two decimal points.

To obtain the distribution of the normal stresses at the interface, the principal stresses expressed in equation (7) are separated by the "shear difference method." This method is based upon expressing the integration of the differential equations of equilibrium in a difference form:

$$(\sigma_x)_B = (\sigma_x)_A - \sum_{i=1}^{n} \frac{(\tau_{xy})_i}{(\Delta y)_i} (\Delta x)_i \tag{8}$$

$$(\sigma_y)_B = (\sigma_y)_A - \sum_{i=1}^{n} \frac{(\tau_{xy})_i}{(\Delta x)_i} (\Delta x)_i \tag{9}$$

Since the values for τ_{xy} are obtained from the shear stresses along two lines drawn on either side of the line under consideration, the contact pressure distributions were calculated along a line 0.040 in. from the interface. The shear stresses, substituted in equations (8) and (9) were obtained from the isoclinic and isochromatic data:

$$\tau_{xy} = (\sigma_x - \sigma_y)/2 \sin 2\theta \tag{10}$$

Comparison of the applied load to the integration of the contact pressure distribution provided a check on the experimental results.

Results and Discussion

More than 50 sets of experiments were performed [35] in order to obtain a comprehensive description of the influence of the geometric parameters of contacting bodies on the contact pressure distribution. While maintaining a contact length l of 1.0 in. (25.4 mm) and changing the height of the upper specimen h between 0.5 in. (12.7 mm) and 3.0 in. (76.2 mm), the dimensions W and H of the lower specimen has been varied between 3 and 5 in. (76.2 and 127 mm). A parametric evaluation indicated that a lower specimen of 3×3 in. (76.2×76.2 mm) can be used to simulate the sought-for effect.

Some of the results obtained from the photoelastic analysis are given in Fig. 6. The isoclinic lines obtained for the case $h/l = 0.5$ (Fig. 6(a)) are bending outwards indicating a stress concentration at the center of the contact. The change in the distribution of the contact pressure as the rigidity of the upper specimen is increased (by changing h/l from 0.5 to 2.5) is clearly visible in Fig. 6(d). The figure shows clearly the high stress concentration at the end points of the contact. These stress concentrations manifest themselves by the subsidiary loops originating at the end points.

The different distributions of contact pressure $p_c\{x\}$ obtained for h/l ratios ranging from 0.5 to 2.5, normalized with respect to the average applied pressure, are compiled in Fig. 7. The graph shows the significant change in the elastic response behavior of the system, and consequently the distribution $p_c\{x\}$, with the variation in h/l.

The contact pressure distribution obtained for $h/l = 2.0$ is very close to the case $h/l = 2.5$ and is omitted from Fig. 7 for clarity. Therefore it can be concluded that the upper specimen behaves as a rigid body when $h/l \geq 2.0$. In reference to Fig. 4, it seems that this result is not unexpected, as the conditions of plate rigidity for that particular configuration was obtained at $h/l = 1.38$. The same case of a square plate $l \times l$ resisting on a semi-infinite mass and subjected to a central concentrated load has been studied by Gorbunov et al. [36]. It was concluded that the plate can be considered as a rigid body if

$$\pi l^3 E_m < 8D(1 - \nu^2{}_m) \tag{11}$$

where D is the flexural rigidity of the plate,

$$D = (E_p h^3)/(12(1 - \nu_p^2))$$

Equation (11) is satisfied when $h/l > 1.68$.

To verify the results obtained by the photoelastic analysis, a two-dimensional plane-stress finite element analysis has been carried out, using SOLID SAP-A [37]. The mesh idealization and node arrangement, for the numerical model, are shown in Fig. 5. The model assumes linear elasticity and perfectly flat contacting surfaces. The contact interface has been idealized by a single row of nodes, and thus constraining the contacting surfaces from any relative movement. Due to symmetry, only half of the contacting plates A and B were considered. By definition, the nodes located along the line of symmetry are restricted from horizontal displacement

$$u = 0 \text{ at } x = 0$$

At the base of the lower specimen, the nodes are restricted from horizontal and vertical displacements, u and v, respectively

$$u = v = 0 \quad \text{at} \quad y = 0$$

The finite element results were found to be in good agreement with the photoelastic predictions within ± 8 percent. The distribution of $p_c\{x\}$ obtained for $h/l = 2$ are very close to that of $h/l = 2.5$ in confirmation of the photoelastic observation. A sample comparison between the

photoelastic and the finite elements results for $h/l=0.5$ is shown in Fig. 8.

The photoelastic results suggest that a uniformity in the distribution $p_c\{x\}$ could be obtained at a particular value of h/l falling within the range $1.0<h/l<1.5$. Preliminary investigation of this range shows the critical role of the corners of the upper specimens' contact surface. This effect has been known for a long time since the original work of Mesmer [38, 39]. A slight rounding off at the corners was found to be a successful way of controlling the steep stress gradient underneath the edges of a rigid body pressing an elastic mass [40, 41]. Galin [40] indicated that the theoretically infinite contact pressures drop to zero if the corners are rounded off.

Conclusions

From the present study, the following conclusions can be drawn:

1. Contact pressure distributions $p_c\{x\}$ of distinctively different shapes can practically be generated by controlling the geometric parameters of the contacting solids; i.e., their relative flexural rigidity.

2. A finite plate, whose dimensions are not less than three-fold the contact length can simulate a two-dimensional rigid base or semi-infinite elastic mass (in contact with a flexible- or rigid-beam, respectively).

3. A variation of the beam height-to-contact length ratio in the range $0.5<h/l<2.0$ causes a significant change in its elastic response behavior – from a flexible to a rigid body. For $h/l>2.0$, the changes in the distribution $p_c\{x\}$ are not significant, and as such, a ratio of $h/l=2.0$ can be taken as the limit for attaining a rigid strip.

Acknowledgment

The work presented in this paper was conducted under the support of the Natural Sciences and Engineering Research Council of Canada, which the authors greatly appreciate.

References

1 Kamiskaya, V., Levina, Z. M., and Reshetov, D. N., "Bodies and Body Components of Metal-Cutting Machine Tools—Calculation and Design," Vols. 1 and 2, National Lending Library for Science and Technology, Boston, Spa., Yorkshire, England, 1964.

2 Koenigsberger, F., *Design Principles of Metal-Cutting Machine Tools*, MacMillan Co., N. Y., 1964.

3 Thornley, R. H., Connolly, R., Barash, M. M., and Koenigsberger, F., "The Effect of Surface Topography Upon the Static Stiffness of Machine Tool Joints," *Int. J. Mach. Tool Des. Res.*, Vol. 5, 1965, pp. 57-74.

4 Yoshida, Y., Honda, F., and Kubota, M., "Thermal Deformation of a Knee-Type Vertical Milling Machine," *Proc. 5th Int. MTDR Conference*, MacMillan Press, 1964, pp. 117-134.

5 Attia, M. H., and Kops, L., "Concept of Thermoelastic Interactions at Machine Tool Joints—A Basis for Improved Machining Accuracy," *Manufacturing Solutions Based on Engineering Science*, edited by Kops, L., ASME, PED—Vol. 3, 1981, pp. 121-149.

6 Attia, M. H., and Kops, L., "On the Role of Fixed Joints in Thermal Deformation of Machine Tool Structures," *Annals of the CIRP*, Vol. 27/1, 1978, pp. 305-310.

7 Attia, M. H., and Kops, L., "Important of Contact Pressure Distribution on Heat Transfer in Structural Joints of Machine Tools," ASME JOURNAL OF ENGINEERING FOR INDUSTRY, Vol. 102, 1980, pp. 159-167.

8 Attia, M. H., and Kops, L., "Nonlinear Thermoelastic Behaviour of Structural Joints—Solution to a Missing Link for Prediction of Thermal Deformation of Machine Tools," ASME JOURNAL OF ENGINEERING FOR INDUSTRY, Vol. 101, 1979, pp. 348-354.

9 Attia, M. H., and Kops, L., "Significance of Structural Joints in Thermal Deformation of Machine Tools," 7th North American Metalworking Research Conference Proc., Manuf. Engrg. Trans., ASME, May 1979, pp. 222-227.

10 Attia, M. H., and Kops, L., "System Approach to the Thermal Behaviour and Deformation of Machine Tool Structures in Response to the Effect of Fixed Joints," *Trans.* ASME JOURNAL OF ENGINEERING FOR INDUSTRY, Vol. 103, 1981, pp. 67-72.

11 Yoshida, Y., "Research on Thermal Deformation of a Vertical Milling Machine," Tech. Report of Mech. Engrg. Lab. No. 82, Tokyo Univ., Tokyo, Japan, 1975.

12 Attia, M. H., and Kops, L., "Computer Simulation of Nonlinear Thermoelastic Behaviour of a Joint in Machine Tool Structure and its Effect on Thermal Deformation," ASME JOURNAL OF ENGINEERING FOR INDUSTRY, Aug. 1979, pp. 355-361.

13 Attia, M. H., and Kops, L., "A New Method for Determining the Thermal Contact Resistance at Machine Tool Joints," *Annals of the CIRP*, Vol. 30/1, 1981, pp. 259-264.

14 Johnson, K. L., "Energy Dissipation at Spherical Surfaces in Contact Transmitting Oscillating Forces," *J. Mech. Engrg. Science*, Vol. 3, No. 4, 1961, pp. 362-368.

15 Johnson, K. L., and O'Connor, J. J., "Mechanics of Fretting," *Proc. Instn. Mech. Engrs.*, Vol. 178, Part 3, 1963-1964, pp. 7-21.

16 O'Connor, J. J., "The Role of Elastic Stress Analysis in the Interpretation of Fretting Fatigue Failures," *Fretting Fatigue*, edited by Waterhouse, R. B., Applied Science Publishers, London, 1981, pp. 23-66.

17 Engel, P. A., and Adams, C. E., "Rolling Wear Study of Misaligned Cylindrical Contacts," *Proc. Int. Conf. on Wear of Materials*, 1979, pp. 181-191.

18 Krause, H., and Senuma, T., "A Contribution Towards Improving the Applicability of Laboratory Wear Tests in Practice," *Proc. Int. Conf. on Wear of Materials*, 1981, pp. 753-763.

19 Czichos, H., "Tribology: Scope and Future Directions of Friction and Wear Research," *J. of Metals*, Sept. 1983, pp. 18-20.

20 Czichos, H., "Current Aspects of Tribology," *Wear*, Vol. 77, 1982, pp. 1-11.

21 Rice, S. L., Nowotny, H., and Wayne, S. F., "The Role of Specimen Stiffness in Sliding and Impact Wear," *Wear*, Vol. 77, 1982, pp. 13-28.

22 Fedotova, A. A., "Wear of Elastic Plane by Beam With Variable Bending Stiffness," *Soviet Journal of Friction and Wear*, Vol. 4, No. 2, 1983, pp. 64-67.

23 Kimura, Y., "Fracture Theory of Wear," *Fundamentals of Tribology*, edited by Suh, N. P. and Saka, N., The MIT Press, 1978, pp. 597-604.

24 Hills, D. A., Ashelby, D. W., and Waterhouse, R. B., "The Physical Influence of Surface Treatment on Wear," *Proc. Int. Conf. on Wear of Materials*, 1979, pp. 396-402.

25 Timoshenko, S. P., and Goodier, J. N., *Theory of Elasticity*, McGraw-Hill, 3rd Edition, 1970, pp. 97-104.

26 Sadowsky, M., "Zweidimensionale Probleme der Elastizitatstheorie," *Ztschr. f. angew. Math. und Mech.*, Band 8, Heft 2, Apr. 1928, pp. 107-121.

27 Goodier, J. N., "Compression of Rectangular Blocks, and the Bending of Beams by Non-Linear Distributions of Bending Forces," ASME *Journal of Applied Mechanics*, Vol. 54, 1932, pp. 173-183.

28 Pickett, G., "Application of the Fourier Method to the Solution of Certain Boundary Problems in the Theory of Elasticity," ASME *Journal of Applied Mechanics*, Vol. 66, 1944, pp. 176-182.

29 Coker, E. G., and Filon, L. N., *A Treatise on Photoelasticity*, Cambridge University Press, 1957, pp. 436-438.

30 Theocaris, P. S., "The Stress Distribution in a Semi-Infinite Strip Subjected to a Concentrated Load," ASME *Journal of Applied Mechanics*, Sept. 1959, pp. 401-406.

31 Cheung, Y. K., and Zienkiewicz, O. C., "Plates and Tanks on Elastic Foundation—An Application of Finite Element Method," *Int. J. Solids Structures*, Vol. 1, pp. 451-461, 1965.

32 Frocht, M. M., *Photoelasticity*, Wiley, Vol. 2, 1948, pp. 19-21.

33 Dundurs, J., and Stippes, M., "Role of Elastic Constants in Certain Contact Problems," *Mechanics*, edited by C. Niels, American Academy of Mechanics, pp. 267-272, 1971.

34 Dally, J. W., and Riley, W. F., *Experimental Stress Analysis*, McGraw-Hill, 1978, pp. 457-459.

35 Al-Kahwati, M., "Study of the Effect of the Relative Dimensions of Two Bodies in Contact on the Distribution of the Contact Pressure," M. E. Project, McGill University, Nov. 1979.

36 Poulos, H. G., and Davis, E. H., *Elastic Solutions for Solid and Rock Mechanics*, Wiley, 1974, p. 260.

37 Wilson, E. L., "SOLID SAP—A Static Analysis Program for Three Dimensional Solid Structures," Structural Engineering Laboratory Report No UC SESM-17-19, Dept Civil Engineering, Univ. of California, Berkeley, Calif., Dec. 1972.

38 Mesmer, G., "Vergleichende Spannungsoptische Untersuchungen und Fliess-Versuche under Kozentrierten Druck," *Z. f. tech. Mech. und Thermodyn.*, Vol. 1, Nos 2 and 3, V.D.I., Berlin, 1930.

39 Mesmer, G., "Personal Communication," June 1976.

40 Galin, L. A., "Contact Problems in the Theory of Elasticity," translated from the Russian by Moss, H., Dept. of Math., North Carolina State College, Oct. 1961.

41 Goodier, J. N., and Loutzenheiser, C. B., "Pressure Peaks at the Ends of Plane Strain Rigid Die Contacts (Elastic)," ASME *Journal of Applied Mechanics*, June 1965, pp. 462-463.